

AERODYNAMICS AND MASS TRANSFER FOR A JET ENTERING A FLUIDIZED BED

N. A. Shakhova* and V. K. Lukashev

UDC 66.096.5

Gas transport is examined for a jet entering a fluidized bed without the production of a gas space; the aerodynamic parameters of the jet are examined.

A jet entering a fluidized bed at a low velocity produces no empty space, since the gas infiltrates the gaps between the particles [1]. The particles are then not entrained by the jet, but instead the mobility is determined by the main flow of fluidizing agent. Research on such jets is essential to the analysis of gas-distributing devices and to the description of processes in fluidized beds generally.

Our measurements on mass transport in such a jet were made with a system of diameter 263 mm in which the center of the gas-distributing grid was fitted with a jet of diameter 4 mm. This was supplied with an air-CO₂ mixture, and the concentration pattern was measured with a sampler leading to a KhL-69 chromatograph. The error of measurement did not exceed 2%. Samples were taken via a 0.8 mm × 0.2-mm tube, which was moved in three mutually perpendicular directions by a coordinate mechanism.

The measurements were made with the following parameters for the jet and bed. The lower limit to the jet velocity was 3.4 m/sec. The upper limit was fixed by the onset of circulation [1], where an empty gas space is produced. The velocity was calculated from the flow rate, which was recorded with a rotameter having a maximum error of 2.7%. The mass concentration of the CO₂ in the mixture was in the range 0.12-1.0 kg of CO₂ per kg of mixture. The height of the bed ranged from 50 to 170 mm. The fluidization number in all cases was $W = 1$. The solid material was granular polystyrene of narrow size range (the average diameter ranged from 2 to 7 mm). The particles were monolithic, so adsorption was negligible.

The measurements were made in the steady state, and the CO₂ concentrations along the axis and in transverse sections fell steadily away from the nozzle (Figs. 1 and 2). However, the concentration at the axis did not fall to that in the bed generally. The concentration in a transverse section varied from a maximum at the axis of the jet to the level in the layer.

Affine behavior was found on processing the curves (Fig. 2b); the following approximation applies for the concentration pattern in a section:

*Deceased.

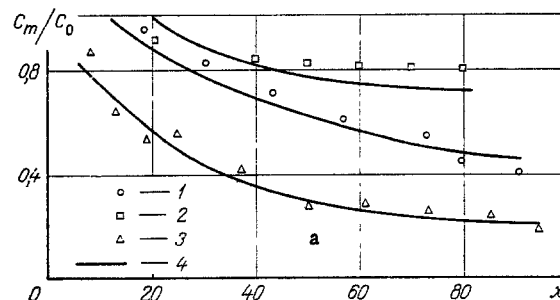


Fig. 1. Variation in CO₂ concentration along the axis of the jet: 1) $d_e = 2.24$ mm, $U_0 = 3.43$ m/sec; 2) 2.24 and 23.4; 3) 3.24 and 3.43; 4) calculation from (6); x in mm.

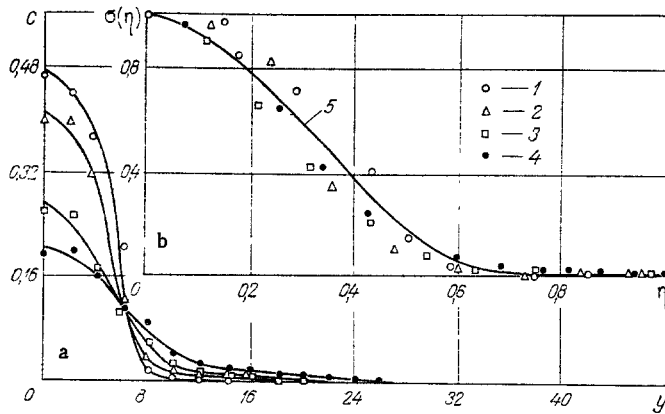


Fig. 2

Fig. 2. Variation in CO₂ concentration in sections of the jet ($U_0 = 3.43$ m/sec, $d_e = 2.24$ mm, (y in mm and C in kg of CO₂ per kg of mixture): 1) $x = 7$ mm; 2) 25; 3) 49; 4) 73; 5) calculation from (1).

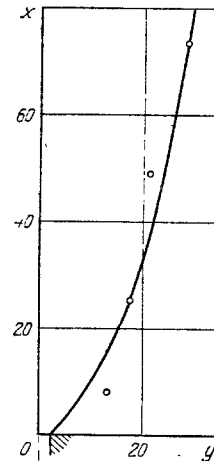


Fig. 3

Fig. 3. Concentration boundary of the jet ($U_0 = 3.43$ m/sec, $d_e = 2.24$ mm, $d_0 = 4$ mm, $C_0 = 0.32$ kg CO₂/kg of mixture; x, y , mm).

$$\sigma(\eta) = [Z(\eta)]^{5/2}, \quad (1)$$

where $Z(\eta)$ is the dimensionless velocity distribution, which is described by the series derived in [2]. We found that there was not greater than 6% error in truncating the series to the following term:

$$Z(\eta) = 1 - 3\eta^2 + 2\eta^3. \quad (2)$$

The effective concentration boundary of the jet could be deduced from the distribution (Fig. 3); the concentration radius is defined as the abscissa of the point on the curve at which the concentration corresponds to the value in the bed (here zero). This method of defining the concentration radius is only approximate because the tail of the curve (Fig. 2) falls slowly. Our curves were truncated at the concentration corresponding to 1% of that at the axis. Experiment indicated that this estimate for the concentration radius was quite sufficient for the determination of integral characteristics.

We also examined the effects of some parameters on the concentration variation along the axis; the rate of fall of the concentration increased with the equivalent diameter of the particles (Fig. 1), but a difference from a jet with a free gas phase [1] was that here the rate of fall decreased as the flow velocity increased (Fig. 1). The initial concentration had no effect on the mass transfer, nor was there any detectable effect from the depth of the bed.

The experimental data were processed on the basis that the excess content of the component is constant in the various cross sections, which is widely used in the analysis of mass transfer in jets [3]; this condition is put for our case as

$$2\pi\epsilon\rho_g \int_0^b U(C - C_b) y dy = \pi r_0^2 U_0 \rho_g (C_0 - C_b). \quad (3)$$

If (3) is reduced to dimensionless form and then transformed, we obtain the axial concentration as

$$\frac{C_m}{C_0} = \frac{1}{2Be} \frac{U_0 r_0^2}{U_m b_d^2} \left(1 - \frac{C_b}{C_0}\right) + \frac{C_b}{C_0}, \quad (4)$$

where

$$B = \int_0^1 \frac{U}{U_m} \sigma(\eta) d\eta.$$

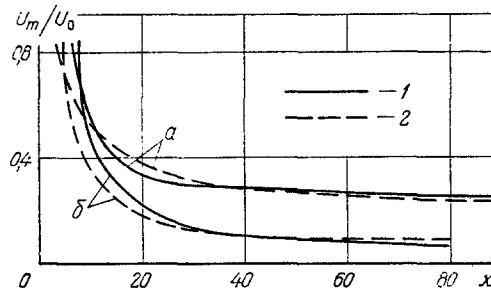


Fig. 4. Variation in velocity at the axis of the jet ($d_e = 2.24$ mm) for U_0 (m/sec) of 3.43 (a) and 23.4 (b): 1) calculated from (7); 2) calculated from the concentration via (6).

The integral B was calculated for known velocity and concentration distributions; these were derived from (1) and (2). Integration gave

$$B = 0.119m + 0.052, \quad (5)$$

where $m = U_b/U_m$.

If there is no gas component in the fluidized bed ($C_b = 0$), (4) simplifies to

$$\frac{C_m}{C_0} = \frac{1}{2Be} \frac{U_0 r_0^2}{U_m b_d^2}. \quad (6)$$

Figure 1 compares calculations from (6) with the measurements; the agreement is good. The concentration radius b_d used in these calculations was determined directly from experiment.

Equations (4) and (6) also allow one to evaluate the aerodynamic characteristics of the jet; direct measurement of the local gas velocity in such a jet is difficult, on account of the low dynamic pressure and the high particle concentration. We now consider an indirect method of determining the speed at the axis.

The gas in the jet entering the fluidized bed is inert with respect to the solid, so the concentration may be measured at the axis and in transverse sections; the concentration curves define the concentration boundary. The concentration at the axis is used with the concentration radius in (6) for each section to calculate the velocity at the axis; the results are used in plotting $U_m/U_0 = f(x)$ (Fig. 4).

On the other hand, the velocity at the axis can be calculated from a published relationship [2], which can be simplified to

$$U_m = \frac{r_0}{b} \sqrt{\frac{U_0(U_0 - U_b)}{2A}}, \quad (7)$$

where

$$A = \frac{3}{35} (1 - m)^2 + \frac{3}{20} m(1 - m).$$

The dynamic radius appearing in (7) is [2] given by

$$b = 4.5x \frac{1 - m}{1 + m}. \quad (8)$$

We can simplify (7) and (8) by using (2) together with the assumption that the particles are not entrained by the flow, as well as that the velocity at the boundary of the jet is equal to that in the system generally ($U_b = U_E$). If κ is measured, we can use (7) and (8) to calculate the speed at the axis and to plot $U_m/U_0 = f(x)$.

The experimental value for the coefficient was derived by comparing the $U_m/U_0 = f(x)$ curves derived from the CO_2 concentrations with calculations from (7) (Fig. 4). We found that this coefficient was independent of the jet velocity. Figure 4 shows curves for the velocity at the axis for jets entering the bed with velocities of 3.4 and 23.4 m/sec, the other parameters being constant. In both cases we found that κ was about 0.35.

Further, κ is inversely related to the particle diameter; for example, a jet of velocity 3.43 m/sec showed a fall in κ from 0.35 to 0.15 as the equivalent diameter increased from 2.24 to 5.92 mm. Therefore, this coefficient is independent of the velocity but is dependent on the characteristics of the bed under these conditions.

NOTATION

b, b_d	are the concentration and dynamic radii of jet;
$C, C_0, C_m,$ C_b	are the mass concentrations in the gas phase: current, initial, on the axis, and at the boundary;
d_0, d_e	are the packing diameter and equivalent diameter of solid particles;
r_0	is the radius of packing;
$U, U_0, U_m,$ U_b	are the velocities: current, initial, on the axis, and at the boundary;
x	is the longitudinal coordinate;
y	is the transverse coordinate;
ε	is the porosity;
ρ_g	is the gas density;
κ	is the experimental coefficient;
$\sigma = (C - C_b) /$ $(C_m - C_b)$	is the dimensionless concentration;
$Z = (U - U_b) /$ $(U_m - U_b)$	is the dimensionless velocity;
$\eta = y/b$	is the dimensionless transverse coordinate.

LITERATURE CITED

1. N. A. Shakhova and V. K. Lukashev, Abstracts of the "Thermiya-75" All-Union Conference [in Russian], Leningrad (1975).
2. N. A. Shakhova and V. K. Lukashev, *Teor. Osn. Khim. Tekhnol.*, **9**, No. 2 (1975).
3. G. N. Abramovich, *Theory of Turbulent Jets* [in Russian], Fizmatgiz, Moscow (1960).

ALLOWANCE FOR THE THERMAL BOUNDARY LAYER AND DIFFRACTION EFFECTS IN DETERMINING THE TRANSIT TIME OF SOUND IN ULTRASONIC FLOWMETERS

I. A. Kolmakov, N. N. Antonov,
and I. A. Logvinov

UDC 536.2.242:534.24

The transit time of sound in ultrasonic flowmeters is investigated with allowance for the thermal boundary layer and diffraction effects.

In determining the time t_t in ultrasonic flowmeters, which is equal to the difference between the downstream and upstream transit times of sound, it is assumed that the temperature of the liquid is constant over the entire path from the source to the receiver. In real situations the liquid flowing in the duct often has a temperature other than that of the duct wall. In this case we know [1-3] that a thermal boundary layer is formed, in which there is a certain temperature distribution and outside of which the liquid temperature is roughly constant and equal to the temperature at the duct entry (Fig. 1). Under these conditions the velocity of sound propagation varies as a function of the temperature zone through which the sound wave passes. At

Translated from *Inzhenerno-Fizicheskii Zhurnal*, Vol. 35, No. 3, pp. 437-444, September, 1978. Original article submitted July 4, 1977.